Check for updates

AGU ADVANCING EARTH AND SPACE SCIENCES

Geophysical Research Letters

RESEARCH LETTER
10.1029/2025GL119138

Understanding the Climate Response to Different Vertical Patterns of Radiative Forcing

An-Zhuo Dai[1], Jonathan Gregory[2,3], and Paulo Ceppi[1]

[1]Department of Physics, Imperial College London, London, UK, [2]National Centre for Atmospheric Science, University of Reading, Reading, UK, [3]Met Office Hadley Centre, Exeter, UK

Key Points:

- Cloud radiative feedback is more negative for forcing at higher altitude
- Differences in feedbacks can be explained by the pattern effect of surface warming
- The vertical structure of forcing affects the pattern of surface warming through altering deep convection

Supporting Information:

Supporting Information may be found in the online version of this article.

Correspondence to:

A.-Z. Dai,
anzhuo.dai16@imperial.ac.uk

Citation:

Dai, A.-Z., Gregory, J., & Ceppi, P. (2026). Understanding the climate response to different vertical patterns of radiative forcing. *Geophysical Research Letters*, *53*, e2025GL119138. https://doi.org/10.1029/2025GL119138

Received 5 SEP 2025
Accepted 8 DEC 2025

Abstract The dependence of climate response on the vertical structure of radiative forcing is studied using a set of idealized experiments, with horizontally uniform and vertically confined forcings. We find for a given effective forcing magnitude, higher-altitude forcing causes a smaller global warming, owing to more negative cloud feedback. We present novel evidence relating this altitude dependence to sea-surface temperature patterns and tropospheric static stability. The imposed instantaneous forcings are horizontally uniform, but higher-altitude forcings more effectively suppress convection in the tropical warm pool, producing a more positive effective (adjusted) surface forcing in that region. This gives rise, during the subsequent climate change, to greater warming contrast between the warm pool and rest of the globe, and hence to increase in low cloud amount. Our results show that to achieve accurate climate projections under anthropogenic forcings, it is important to correctly represent the vertical structures of the applied radiative forcing.

Plain Language Summary Climate change is driven by changes in the Earth's energy balance, known as radiative forcing. Previous studies have shown that the extent of global warming depends on both the magnitude and geographic pattern of forcing. Using global climate model experiments, we find that forcings at higher altitudes lead to weaker global warming than those closer to the surface. This difference can be explained by the patterns of surface warming and the resulting changes in low-cloud amount. We also hypothesize that the different warming patterns between forcing altitudes are likely driven by deep-convection changes in the tropics. The findings of this research highlight the need for climate models to accurately represent the vertical distribution of radiative forcing to improve estimates of global warming.

1. Introduction

The linearized global-mean top-of-atmosphere (TOA) energy balance

$$N = F + \lambda \Delta T \tag{1}$$

describes the Earth's net downward TOA radiative flux N, after applying an effective radiative forcing (ERF) F, with ΔT the change in surface air temperature (SAT) with respect to the unperturbed initial steady state, in which $N = 0$ (Cess et al., 1990; Gregory et al., 2004). In this equation, λ is a constant feedback parameter (W m^{-2} K^{-1}), where we follow the sign convention that signifies a stable climate when it is negative. The radiative imbalance causes ΔT to change until a perturbed equilibrium is reached, in which again $N = 0 \Rightarrow \Delta T = -F/\lambda$. Within this forcing-response framework, fast responses that are directly consequent on the applied forcing are known as *rapid adjustments* and usually considered as part of the forcing (Forster et al., 2021; Sherwood et al., 2015). The remaining responses are the feedbacks. They are proportional to ΔT, so we call them "T-mediated." When F is due to doubling the atmospheric CO_2 concentration, ΔT is called the "equilibrium climate sensitivity." For forcings in general, a less negative λ gives a larger "climate sensitivity," meaning a greater equilibrium global-mean warming per unit forcing $\Delta T/F$. For different forcing agents, the variation of λ between agents is the reason for the variation in the "forcing efficacy" (Hansen et al., 2005; Richardson et al., 2019). The efficacy is the ratio of λ under CO_2 forcing to λ for the agent in question, where a less negative λ means higher efficacy.

The linear conceptual model in Equation 1 has been shown to provide an excellent representation of the climate response to realistic forcings and is widely used to quantify climate feedbacks in coupled climate models and observations to help constrain the amount of future global warming (Caldwell et al., 2018; Ceppi & Nowack, 2021; Knutti et al., 2017; Meyssignac et al., 2023; Vial et al., 2013). Despite its strengths, however, this

© 2025. The Author(s).
This is an open access article under the terms of the Creative Commons Attribution License, which permits use, distribution and reproduction in any medium, provided the original work is properly cited.

19448007, 2026, 1, Downloaded from https://agupubs.onlinelibrary.wiley.com/doi/10.1029/2025GL119138 by Imperial College London, Wiley Online Library on [21/10/2026]. See the Terms and Conditions (https://onlinelibrary.wiley.com/terms-and-conditions) on Wiley Online Library for rules of use; OA articles are governed by the applicable Creative Commons License

model is deficient in that it does not take into account the effects of the spatial pattern of temperature change (Andrews & Webb, 2018; Ceppi & Gregory, 2017; Gregory & Andrews, 2016; Zhou et al., 2016). It has become increasingly recognized that the strength of climate feedbacks is driven not only by the global-mean magnitude of surface warming, but depends also upon the geographical pattern of sea-surface temperature (SST) change; this is known as the *pattern effect* (Andrews & Webb, 2018; Andrews et al., 2015; Bloch-Johnson et al., 2020; Dong et al., 2019; Rugenstein et al., 2020; Stevens et al., 2016).

The energy balance model framework was refined by Ceppi and Gregory (2019) to incorporate global-mean tropospheric stability change ΔS as another term on which N depends, as well as F and ΔT. They hypothesized that the pattern effect operates via ΔS, which is a strong controlling factor for change in cloud and hence cloud radiative effect (CRE) (Klein et al., 2017; Qu et al., 2015; Wilson Kemsley et al., 2024). They showed that differences in λ among realistic forcing agents are largely due to low-cloud responses to ΔS, in turn driven by changes in the underlying SST response patterns. The theory of Ceppi and Gregory (2019) provides an explanation for the relationships between forcings and their elicited feedbacks that have been characterized by a range of other studies (Hansen et al., 2005; Marvel et al., 2016; Modak & Bala, 2019; Modak et al., 2016; Salvi et al., 2022; Shindell, 2014).

While several studies have considered the impact of the horizontal distribution of ERF on climate feedback (Ceppi & Gregory, 2019; Günther et al., 2022; Liu, Lu, Garuba, Huang, et al., 2018; Salvi et al., 2022), the impact of the vertical forcing profile has received comparatively little attention (Salvi et al., 2022). Species such as black carbon, sulfate aerosol, and carbon dioxide have been shown to differ significantly in their vertical direct radiative forcing profiles (Salvi et al., 2021; Samset & Myhre, 2011). Furthermore, their relative concentration has varied in the past and will change in the future (Lee et al., 2021). The link between the vertical pattern of radiative forcing and the resulting climate change constitutes a gap in our understanding of climate dynamics, which in this work we aim to fill, in order to help constrain estimates of climate sensitivity.

2. Models and Methods

The simulations used for this study were performed using the Community Earth System Model 2 (CESM2) with a CAM4 atmosphere, both alone and coupled to a slab ocean, as well as the Hadley Centre Coupled Model version 3 (HadCM3) family of general circulation models (GCM), which includes the atmosphere-only configuration HadAM3 and atmosphere–slab configuration HadSM3. A slab ocean model was chosen over a dynamic ocean as it is computationally cheaper, hence permitting more and longer experiments. This advantage comes with the disadvantage of being unable to account for changes in oceanic processes that help shape the surface warming pattern. We will further discuss the implications of this choice of ocean model later in Section 4. A $1.9° \times 2.5°$ grid resolution was used for CESM2 and $3.75° \times 2.5°$ for HadSM3.

Given that this study is concerned with the dependence of climate responses on the altitude of radiative forcing, but not its geographical pattern, we opted to use idealized, horizontally uniform "ghost" forcings (Hansen et al., 1997), instead of realistic physical forcing agents. These ghost forcings are vertically confined heating anomalies, fixed for the entire duration of the simulations. The vertical structures of these forcings differ slightly between those used in CESM2 and HadAM/SM3. For CESM2, their structures are shown in Figure 1a following those used by Salvi et al. (2021). They are centered on 875, 750, 625, 500, and 375 hPa, and vertically integrate to 2 W m^{-2}. HadAM3/SM3 used forcings with 7 W m^{-2} (approximately the global-mean ERF from quadrupling CO_2 in this model) located in single model (hybrid sigma–pressure) layers, located at 870, 700, 500, and 300 hPa (Figure 1b). Note that for Figure 1b, the profiles all vertically integrate to the same value, but have differing magnitudes to account for the thickness of the individual model layers. Here on we refer to these idealized forcings as *instantaneous ghost forcings* (IGF) to differentiate from the ERF values. Both forcing structures and magnitudes were tested and the responses showed little difference (not shown), thus allowing the results to be compared between the two models.

The pressure levels range from the planetary boundary layer to the upper free troposphere. For ease of comparison, from here on we refer to the experiments with forcings centered on 875 hPa for CESM2, and 870 hPa on HadAM3/SM3, as the lower-tropospheric forcing (LTF) cases. Similarly, the CESM2 375 hPa and HadCM3 300 hPa cases are referred to as the upper-tropospheric forcing (UTF) cases.

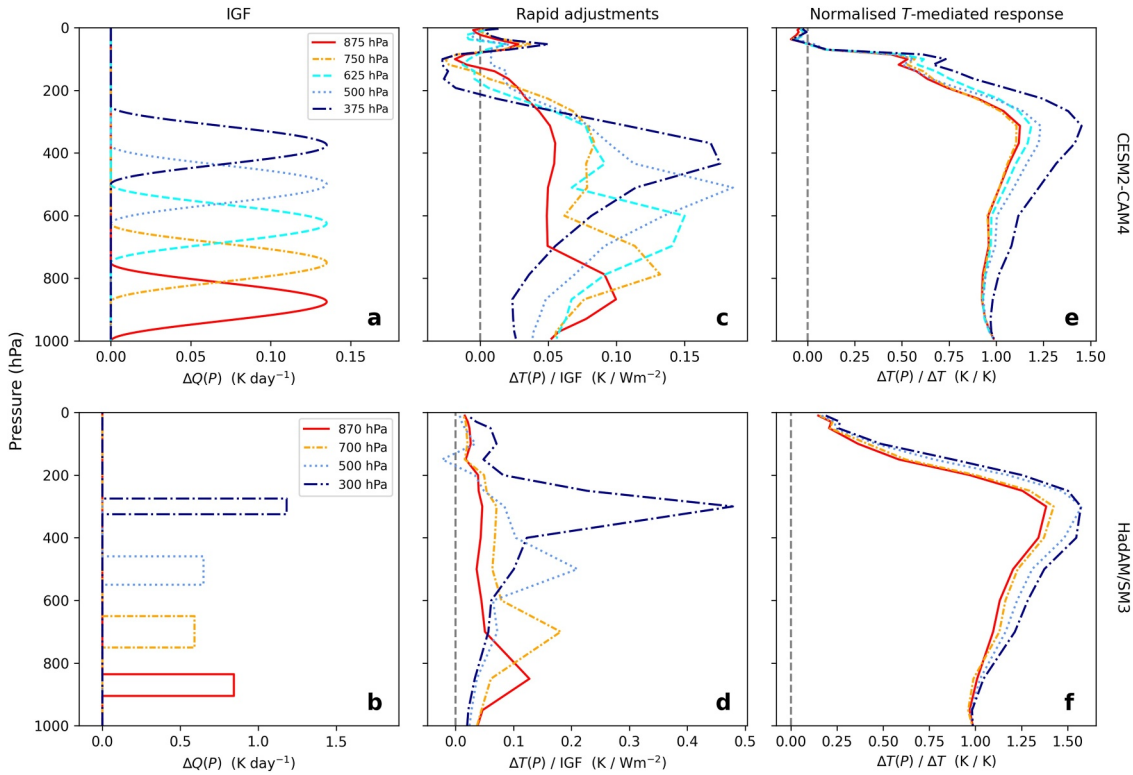


Figure 1. Applied "ghost" forcing and equilibrium global-mean temperature response profiles for CESM2 (top row) and HadAM/SM3 (bottom row). (a, b) Forcing vertical profiles, calculated in the models as additional heating ΔQ. (c, d) Responses due to rapid adjustments normalized by the instantaneous ghost forcings for the corresponding model. (e, f) T-mediated responses normalized by equilibrium average surface warming.

The perturbed atmosphere–slab simulations branched from equilibrated control runs, and were run for 60 years for CESM2 and 50 years for HadSM3 (Figures S1 and S2 in Supporting Information S1), reaching perturbed equilibria within about 25 years, this being the timescale set by the thermal inertia of the slab. We refer to the period before equilibrium is reached as the "transient" phase. We quantify equilibrium climate change as the difference between the time-mean of the equilibrium period (year 26–end) and the long-term control time-mean. We define the "warming pattern" ΔT_p as the perturbed equilibrium field of global-mean SAT change, divided by ΔT, its global mean.

We designate subscripts to denote any variable X at equilibrium in the perturbed and control runs of the slab model as X_{pert} and X_{ctl}. The slab model response to the applied forcing is then $\Delta X = X_{\text{pert}} - X_{\text{ctl}}$. Like Ceppi and Gregory (2019), we follow the Hansen et al. (1997) method of quantifying the contribution of rapid adjustments to ΔX, using output from atmosphere-only simulations for forcing at each pressure level. The atmosphere-only simulations were performed with prescribed 12-month repeating SST and sea ice concentration climatologies obtained from the slab control runs. By this means, they prevent surface temperature change over the ice-free ocean (although not over land), and hence mostly suppress the feedbacks, which are proportional to ΔT (Equation 1); the radiative response is dominated by the adjustments, which are caused by the forcing directly. The atmosphere-only simulations equilibrate approximately within a year, the timescale set by the atmosphere, land and sea-ice surface, and were run for 20 years on CESM2 and 30 years on HadAM3.

We denote the equilibrium change of X in the atmosphere-only runs as $X_{\text{atm,pert}}$ and $X_{\text{atm,ctl}}$. Hence we can separate the slab ΔX into the adjustment $\Delta X_{\text{adj}} = X_{\text{atm,pert}} - X_{\text{atm,ctl}}$, and the T-mediated remainder ΔX_{T}. Putting together the definitions gives:

$$\Delta X_{\text{T}} = \Delta X - \Delta X_{\text{adj}} = (X_{\text{pert}} - X_{\text{ctl}}) - (X_{\text{atm,pert}} - X_{\text{atm,ctl}}). \quad (2)$$

19448007, 2026, 1, Downloaded from https://agupubs.onlinelibrary.wiley.com/doi/10.1029/2025GL119138 by Imperial College London, Wiley Online Library on [21/10/2026]. See the Terms and Conditions (https://onlinelibrary.wiley.com/terms-and-conditions) on Wiley Online Library for rules of use; OA articles are governed by the applicable Creative Commons License

19448007, 2026, 1, Downloaded from https://agupubs.onlinelibrary.wiley.com/doi/10.1029/2025GL119138 by Imperial College London, Wiley Online Library on [21/10/2026]. See the Terms and Conditions (https://onlinelibrary.wiley.com/terms-and-conditions) on Wiley Online Library for rules of use; OA articles are governed by the applicable Creative Commons License

The drawback of the Hansen method is that the equilibrium of the atmosphere-only simulations is not a physical state which occurs during coupled atmosphere–slab climate change. The Gregory method, on the other hand, uses only the slab transient states, by regressing annual global-mean N against ΔT, from which one can obtain the ERF from the N-intercept and λ from the gradient. A drawback of this method is that it is limited by the length of the transient phase, whereas the atmosphere-only simulations can be run to any length required. For single-member slab model simulations that equilibrate on a decadal timescale, the spin-up period may be too short for accurate results from regression. The global-mean feedbacks and adjustments obtained using both methods are discussed in Section 3.1 below.

To help with understanding the drivers of SST patterns during this study, we examine the energy budgets at the surface after allowing for the atmosphere to adjust to the forcings. This *effective surface forcing* (ESF) is calculated as the sum of net downward radiative and turbulent heat flux anomalies at the surface, with respect to the control climate, due to forcing and adjustment but excluding feedback. In the global mean, ERF and ESF are equal, but they differ locally due to changes in the horizontal transport of sensible and latent heat within the atmosphere (Andrews et al., 2009; Colman, 2015; Ramanathan, 1981; Sejas et al., 2021).

3. Results

The slab equilibrium surface temperature responses (Figures 2a and 2b) show a relationship between the pressure level of the forcing and the consequent climate response. In this section we analyze that relationship, and examine its link to the pattern effect.

3.1. Global-Mean Rapid Adjustment and Feedbacks

We present the equilibrium ΔT and ESF values in Figures 2a and 2b; the Gregory regression results can be found in Figures S3 and S4 in Supporting Information S1. Note that the rapid adjustments can be inferred as the ESF minus the IGF (2 W m^{-2} for CESM2 and 7 W m^{-2} for HadSM3). Although the adjustments from the two methods differ, they agree qualitatively for each model. From the results it can be seen that ESF in CESM2 is smaller than the IGF in nearly all cases, and decreases with increasing forcing altitude that is there is a negative rapid adjustment, of larger magnitude for forcing at greater altitude. This result is consistent with Salvi et al. (2021), using the same GCM, who ascribed the effect to variations in low cloud adjustment. By contrast, in HadSM3 the opposite dependence on forcing altitude is seen; the adjustment is negative at low altitude, positive at high altitude. This is a distinct and interesting discrepancy between the models in the behavior of rapid adjustments in the global mean, whose explanation we will leave for future work as our present focus is on feedbacks.

From the ESF and resultant ΔT, the equilibrium feedback parameter (λ) is calculated as $-\mathrm{ESF}/\Delta T$. Both models produce least negative λ under LTF, and most negative λ for UTF. This relationship is clearest from the Hansen results in Figures 2c and 2d, but is less evident from regression for CESM2 owing to large uncertainties (Figure S3 in Supporting Information S1), although a broad trend can be argued. In HadSM3, the opposite tendencies of ERF and λ with respect to forcing altitude lead to a roughly invariant ΔT, whereas in CESM2 the tendencies are in the same sense and produce a monotonic decrease of ΔT with increasing altitude.

In both models, the majority of the variation in λ comes from cloud feedback, calculated as the change in CRE per unit warming. We expect the clear-sky residual differences to be dominated by lapse-rate feedback, since SST patterns typically have little impact on other longwave non-cloud feedback components (Ceppi & Gregory, 2019) if relative humidity is used as a state variable in the feedback decomposition (Held & Shell, 2012). Figures 1e and 1f show the global-mean T-mediated vertical warming profiles, where the top of the troposphere warms more than the surface across all cases, allowing for additional longwave cooling which constitutes a negative lapse-rate feedback. We found that the residual differences are dominated by shortwave clear-sky feedbacks in CESM2 and can be largely attributed to changes in surface albedo, whereas in HadSM3 longwave clear-sky feedbacks dominate the residual, which we speculate to be due to lapse-rate feedbacks. Any non-linear effects on λ due to warming under different forcing levels are also captured in the residual, an effect expected to be weak in the range of ΔT seen here (Bloch-Johnson et al., 2021; Zhou et al., 2023). Following the same line of reasoning by Ceppi and Gregory (2019), we hypothesize that the feedback differences between forcing altitudes arise as a result of the SST pattern effect.

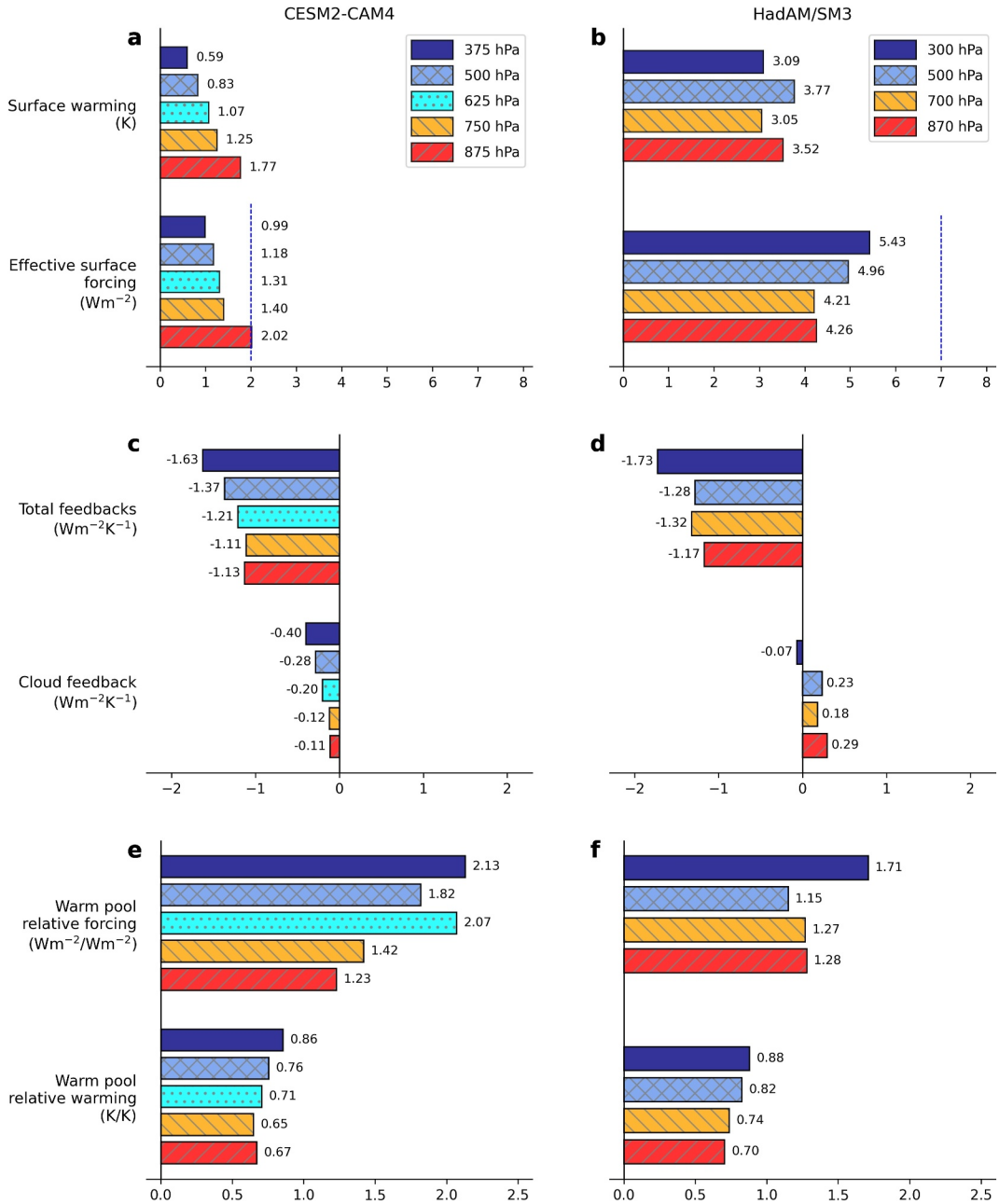


Figure 2. From top to bottom, the globally averaged surface warming response (ΔT) and effective surface forcing; global total (λ) and cloud (λ_{cld}) feedbacks; and the amount of surface forcing (F_{wp}) and warming (ΔT_{wp}) over the warm pool relative to the global average, with the location of the warm pool taken as the warmest 30% of gridpoints between 30°N–30°S from control climatologies (Fueglistaler, 2019). Colors and hatchings represent values from individual perturbed experiments. Dashed lines indicate the magnitudes of the respective instantaneous ghost forcings for each experiment.

3.2. Response Patterns

To investigate the hypothetical role of the pattern effect for changes in climate feedback with forcing altitude, we compare normalized response patterns between models and across quantities. As there are more simulated years in the equilibrium state than the transient, the presented patterns are calculated from the time-mean of the equilibrium period. We define the normalized T-mediated response patterns of any variable X in the slab experiment as the time-mean equilibrium change in the field ΔX divided by ΔT. Similarly, all ESF fields are divided by their global mean values. In Figure 3 we present the ESF and response patterns for the UTF and LTF

19448007, 2026, 1, Downloaded from https://agupubs.onlinelibrary.wiley.com/doi/10.1029/2025GL119138 by Imperial College London, Wiley Online Library on [21/10/2026]. See the Terms and Conditions (https://onlinelibrary.wiley.com/terms-and-conditions) on Wiley Online Library for rules of use; OA articles are governed by the applicable Creative Commons License

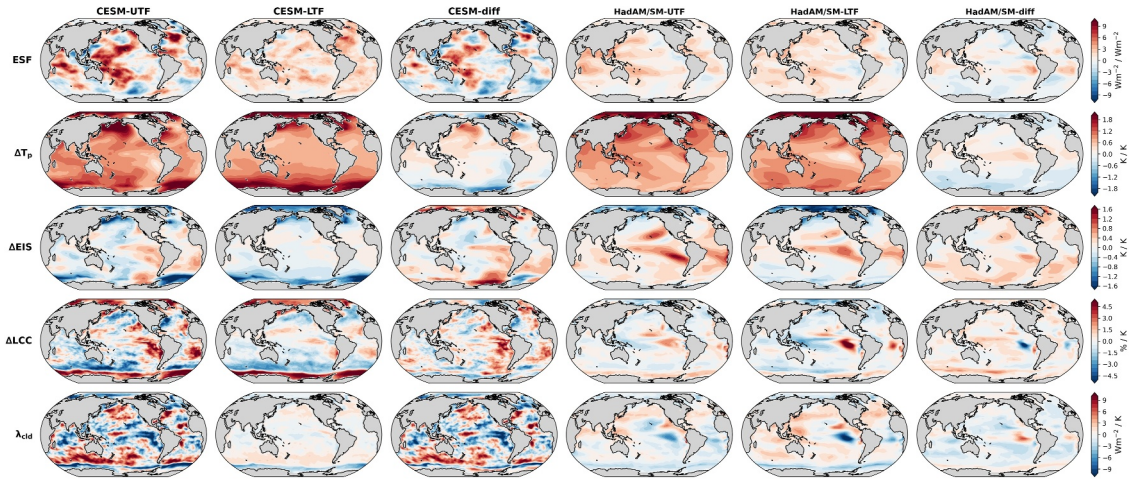


Figure 3. Geographical patterns of forcing and T-mediated responses for CESM2 (left three columns) and HadAM/SM3 (right three columns). Within each group of columns, from left to right shows the response under lower-tropospheric forcing (LTF), response under upper-tropospheric forcing (UTF), and the difference pattern between them, calculated from UTF minus LTF. The top row shows the effective surface forcing (W m^{-2}), with the following showing responses in surface temperature relative to globally averaged warming (ΔT_p, K/K), estimated inversion strength (ΔEIS, K/K), low cloud cover (ΔLCC, %/K), and cloud feedback (λ_{cld}, W m^{-2}/K, which is by definition the change in cloud radiative effect normalized by ΔT).

cases from both models, as well as the difference pattern between the cases. The full set of patterns can be found in Figures S5 and S6 in Supporting Information S1. Being the responses to vertical localized forcings, these patterns could be regarded as Green's functions for estimating the ΔX response to a horizontally uniform forcing of arbitrary vertical structure, similar in spirit to the response functions to geographically localized surface "patch" forcings used by for example, Liu, Lu, Garuba, Leung, et al. (2018) to estimate the response to an arbitrary field of surface forcing.

From Figure 3, the patterns are generally similar between forcing altitudes (Figure 3 columns 1–2 and 4–5) but with UTF producing more pronounced patterns than LTF. Consistent with the above, the difference patterns (columns 3 and 6) tend to resemble the UTF and LTF patterns themselves, especially UTF. These statements are true for all cases except for HadSM3 low cloud responses, which will be discussed later in this section.

The patterns of ESF as obtained by the Hansen method are shown in the top row of Figure 3. From the CESM2 ESF difference pattern, a strong east–west contrast can be seen in the Pacific, with the West Pacific receiving less surface forcing from LTF than UTF, and vice versa for the East Pacific. This pattern is also present, though much weaker, in HadAM3 ESF. Additionally, a tropics–extratropics contrast can be recognized in the ESF difference patterns for both models, where higher-latitude regions generally experience more negative forcing in the UTF case.

Although one may expect a strong correlation between the pattern of ESF and the initial surface warming response in slab-ocean runs, the equilibrium warming can have a different pattern, because the surface warming pattern evolution is shaped by both local and remote feedbacks (e.g., Stuecker et al., 2020). However, certain similarities can be drawn between the first two rows in Figure 3; for example, the tropics–extratropics contrast in ESF is also present in the warming patterns, with UTF favoring more strongly negative extratropical responses. The east–west contrasts in surface forcing and warming patterns across the tropical Pacific also bear qualitative resemblance.

To assess changes in tropospheric stability, which could be associated with the pattern effect, we use the estimated inversion strength (EIS) metric from Wood and Bretherton (2006), which measures the strength of the inversion layer between the planetary boundary layer and the free troposphere. It is calculated from temperatures at 1,000 and 700 hPa, relative to a temperature profile that accounts for moist convection above the lifting condensation level. Because local surface warming has a destabilizing effect on the troposphere, we expect the ΔEIS patterns shown in row 3 of Figure 3 to be anti-correlated with those of ΔT_p in row 2. This is indeed true for the cases shown here, where even regions with weak warming response differences in the tropics also give discernible and opposite ΔEIS differences.

19448007, 2026, 1, Downloaded from https://agupubs.onlinelibrary.wiley.com/doi/10.1029/2025GL119138 by Imperial College London, Wiley Online Library on [21/10/2026]. See the Terms and Conditions (https://onlinelibrary.wiley.com/terms-and-conditions) on Wiley Online Library for rules of use; OA articles are governed by the applicable Creative Commons License

19448007, 2026, 1, Downloaded from https://agupubs.onlinelibrary.wiley.com/doi/10.1029/2025GL119138 by Imperial College London, Wiley Online Library on [21/10/2026]. See the Terms and Conditions (https://onlinelibrary.wiley.com/terms-and-conditions) on Wiley Online Library for rules of use; OA articles are governed by the applicable Creative Commons License

Weaker boundary-layer inversions as indicated by a smaller EIS lead to less cloud formation in the lower levels of the troposphere (Klein & Hartmann, 1993; Wood & Bretherton, 2006). The low-cloud amount difference patterns, calculated from cloud cover between the surface and 700 hPa, reveal that in general the regions with more low cloud under UTF correspond well to the regions with more positive ΔEIS, and vice versa (Figure 3 rows 3–4). As mentioned previously, the individual HadSM3 response patterns to UTF and LTF display the opposite behavior in the tropics to those of CESM2. This may be explained by boundary layer stability not being the only controlling factor of cloud formation (Myers & Norris, 2015). Therefore it is likely that this intermodel difference in ΔLCC response to ΔEIS is caused by differing representations of factors such as atmospheric circulation and moisture transport.

Since higher-level clouds tend to have more neutral net CREs, we can assume that the differences in cloud feedbacks (λ_{cld}) are dominated by changes in low-cloud amounts (Matus & L'Ecuyer, 2017; Zelinka et al., 2012). (The experiments performed in this study did not include satellite simulator output, so that we cannot cleanly decompose λ_{cld} into components due to clouds at different levels.) Comparing the last two rows of Figure 3, from the CESM2 maps we can identify regions in the tropical East Pacific where there are strong increases in low-cloud amount under UTF, with correspondingly more negative λ_{cld}. Similar features can also be identified in the Atlantic and Southern Oceans. Although the HadSM3 results show that the patterns of λ_{cld} is more positive over the East Pacific under UTF than LTF, there still is consistency between the patterns of ΔLCC and λ_{cld}, that is, they are anticorrelated.

3.3. The Role of the Warm Pool and the Pattern Effect

Experiments with patch SST perturbations (Bloch-Johnson et al., 2024; Dong et al., 2019; Liu, Lu, Garuba, Huang, et al., 2018; Zhou et al., 2017) have shown that even small warming differences in regions of deep convection can strongly impact the global energy budget through a pattern effect. It is therefore important to recognize from the CESM2 warming patterns (Figure 3, row 2, columns 1–3) that the Indo-Pacific warm pool warms more per unit globally averaged warming under UTF than LTF, whilst the inverse is true for the East Pacific cold tongue.

Surface warming in the warm pool is effectively communicated aloft to the local free troposphere by deep convection, which then remotely warms the rest of the tropical free troposphere via gravity wave adjustment (Bretherton & Smolarkiewicz, 1989; Sobel & Bretherton, 2000; Williams et al., 2023; Zhang & Fueglistaler, 2020). This causes a negative radiative response from lapse-rate and cloud-radiative changes (Andrews & Webb, 2018; Ceppi & Gregory, 2017; Joshi et al., 2008; Zhou et al., 2016). By contrast, surface warming in tropical subsidence regions is confined to the boundary layer by the strong inversion layer above, giving a positive radiative response.

In order to evaluate the radiative impact of the tropical SST pattern, Fueglistaler (2019) proposed the SST$^{\#}$ metric, calculated as the difference between the warmest 30% of tropical SST and the tropical-mean SST. This metric has been shown to capture much of the variance in shortwave CRE unexplained by changes in the average tropical SST. A more positive SST$^{\#}$ stabilizes the troposphere, causing more low clouds and a more negative cloud feedback, and vice versa.

Whereas SST$^{\#}$ considers the difference between the warm pool and the *tropical* average, we calculate the difference in warming ΔT_{wp} and in forcing F_{wp} over the warm pool relative to the *global* average. From model control outputs, gridpoints representing the warm pool are selected by choosing the warmest 30% of SST between 30°N and 30°S (the same as those used for SST$^{\#}$) before spatially averaging the forcing and temperature response maps over those points. By exploring changes to the warm pool, relative to the rest of the world, under different forcing altitudes, we can highlight its role in driving different global feedbacks, and establish a link between forcing altitude and the resultant surface warming.

The ΔT_{wp} and F_{wp}, for each model and forcing altitude, are shown in Figures 2e and 2f. Note that each quantity is divided by the corresponding global mean, so they are both dimensionless: F_{wp} is the ratio of warm-pool regional-mean ESF to global-mean ESF, and ΔT_{wp} is the warm-pool regional-mean temperature change in K per K of global-mean warming. Enhanced warming in the warm pool is not evident in the maps for HadSM3, where instead a broad tropics-to-extratropics contrast dominates (Figure 3, row 2, columns 4–6). Nonetheless, in these warm

19448007, 2026, 1, Downloaded from https://agupubs.onlinelibrary.wiley.com/doi/10.1029/2025GL119138 by Imperial College London, Wiley Online Library on [21/10/2026]. See the Terms and Conditions (https://onlinelibrary.wiley.com/terms-and-conditions) on Wiley Online Library for rules of use; OA articles are governed by the applicable Creative Commons License

pool metrics, it can be seen that ΔT_{wp} is small under LTF but grows with increasing forcing altitude, for *both* models.

While we do not find a monotonic relationship between F_{wp} and ΔT_{wp} across forcing altitudes, both metrics generally increase as forcing altitude goes up: the warm-pool ESF per unit of global-mean ESF, and the warm-pool warming per unit T, are both larger for UTF than LTF, in both models. This suggests that the surface forcing pattern has some impact on the resulting equilibrium warming pattern, even though the full spatial patterns are only in partial agreement (Figure 3 rows 1–2).

3.4. A Mechanism for Surface Forcing Patterns

Previous authors have demonstrated the important role of the warm pool in the pattern effect, whereby a larger ΔT_{wp} leads to a generally more stable troposphere, more low cloud cover, and a more negative cloud feedback. Here we build on these ideas to suggest a possible explanation for the effects of forcing altitude on the pattern of surface temperature change and the climate feedback (more negative feedback, and lower climate sensitivity, for higher-altitude forcing).

Figures 1c and 1d shows the vertical profile of global-mean temperature change following the rapid adjustment of the atmosphere to the forcing, but before the SSTs have changed. Peak warming is localized at the altitudes where the forcings have been placed, with varying degrees of warming extending above the forcing centers. The maximum magnitude of the temperature adjustment increases with the forcing altitude, because the change in the lapse rate between the surface and the level of maximum warming is similar for all altitudes of forcing. This is even clearer if the vertical profile is plotted in altitude rather than air pressure, putting the lapse rate in K/km, which stretches the vertical axis more toward the TOA (not shown).

It is not obvious why the lapse-rate change (between the surface and the forcing level) is independent of forcing altitude. It is probably related to the change in the atmospheric heat budget during adjustment, whereby the IGF is balanced by reductions to atmospheric radiative convergence and to upward enthalpy (latent and sensible heat) flux from the surface. In each model, the IGF, which is the same at all altitudes, is partitioned in roughly the same way between these two contributions, regardless of forcing altitude. In radiative–convective equilibrium, the balance of these two contributions determines the lapse rate.

This global-mean argument suggests a similar change in convection for all forcing altitudes, and hence does not explain the relationship of F_{wp} to forcing altitude. We hypothesize that deep convection, which occurs predominantly in the warm pool, is particularly sensitive to *high-altitude* warming, which is greatest for UTF (Figures 1e and 1f). If we take the differences in temperature between the top and bottom of the troposphere as a proxy for the stability relevant to warm-pool convection, it follows that UTF has a stronger stabilizing effect than LTF *for deep convection*.

Therefore we propose that, during the adjustment phase, changes in deep convection depend on the forcing altitude. This affects the surface turbulent heat fluxes in the warm pool region: suppressed convection in the UTF case draws less heat away from the surface, causing a more strongly positive local surface energy imbalance that is ESF; the opposite occurs in the LTF case, with enhanced convection. These local imbalances drive the patterns of ESF away from homogeneity, causing F_{wp} under UTF to be larger than under LTF.

In the following T-mediated feedback phase, the SSTs begin by responding to the ESF, which initially is the sole perturbation to the surface energy balance. Although local feedbacks later modify the pattern of surface flux changes, we propose that the larger F_{wp} for UTF than LTF from adjustment causes the larger ΔT_{wp} during the T-mediated phase.

Figures 1e and 1f shows that, for all forcing altitudes, in both models, the global-mean lapse rate throughout the free troposphere decreases during the T-mediated phase. This is a robust outcome of global warming, due to the temperature-dependence of the saturated adiabatic lapse rate. In addition, however, we see that the increase in stability is greater for UTF than LTF. Following previous work, we propose that this difference results from the difference in ΔT_{wp}. Warm-pool warming promotes convection in the warm pool and subsidence elsewhere, with widespread consequences. In particular, the subsidence tends to increase the low-cloud amount worldwide, making CRE more negative. Our proposal suggests that all these effects will be greater per K of global warming in response to UTF than LTF, because of the difference in ΔT_{wp}. Thus we arrive at an explanation whereby higher-

19448007, 2026, 1, Downloaded from https://agupubs.onlinelibrary.wiley.com/doi/10.1029/2025GL119138 by Imperial College London, Wiley Online Library on [21/10/2026]. See the Terms and Conditions (https://onlinelibrary.wiley.com/terms-and-conditions) on Wiley Online Library for rules of use; OA articles are governed by the applicable Creative Commons License

altitude forcing, via greater F_{wp} and ΔT_{wp}, produces more negative cloud feedback in the global mean (Figures 2c and 2d).

Although it is helpful, we have shown that the surface energy flux perspective is not sufficient to explain the equilibrium warming pattern. This is likely because coupled ocean–atmosphere processes shape the evolution of the pattern: the atmospheric response to the initial SST change feeds back on the surface fluxes, which in turn further modifies the warming pattern and thus the atmospheric response. If this is correct, then the initial warming pattern should much more strongly resemble the pattern of ESF. Future work should test this idea, and identify the coupled mechanisms shaping the subsequent evolution of the warming pattern.

4. Conclusion

Radiative forcing agents are characterized by diverse spatial structures of anomalous heating. For example, forcing from black carbon is strongest around the top of the planetary boundary layer and becomes weaker with increasing altitude (Samset & Myhre, 2011), whereas for CO_2 the profile peaks near the surface and decays slowly with altitude (Salvi et al., 2021). How these differences translate into the global climate response remains poorly understood.

Here we provide novel evidence for a clear relationship between the vertical structure of radiative forcing, climate feedbacks, and the resultant global surface temperature change. For higher-altitude forcing, the warm pool warms more, relative to the global average, due to changes in the surface energy budget driving differing patterns of surface warming response. This enhances deep convection over the warm pool, warming the global free troposphere and stabilizing the lower troposphere; this in turn promotes low-cloud growth, causing more strongly negative feedbacks, and thus a lower climate sensitivity.

These links were tested by applying horizontally uniform and vertically confined ghost forcings with equal magnitudes to equilibrated climates in two coupled GCMs with slab oceans (CESM2 and HadSM3). Despite the two models producing SST responses that differ significantly in their global averages and geographical patterns, they both demonstrate similar relationships and operating mechanisms between forcing altitude and feedbacks. They moreover exhibit qualitative similarities in the patterns, which must arise from common behavior of atmospheric processes in response to the forcing, because the forcings themselves are geographically uniform.

We also present a hypothesis which seeks to address the existing knowledge gap in the relationship between the vertical profile of radiative forcing and the warming pattern. By splitting the globally averaged atmospheric response into its atmosphere-only rapid adjustment and T-mediated feedback phases, we are able to identify the role of the tropospheric temperature lapse rate in moderating changes in the warm pool. Forcings at higher altitudes have more stabilizing effects on the troposphere during both phases, but in different ways. We suggest suppression of convection by increased stability during the adjustment phase particularly affects the warm pool, and thereby imprints itself on the pattern of ESF. In the T-mediated phase, by contrast, the increase in stability has a worldwide effect on low-cloud cover. While consistent with our results, some links in our hypothesis are conjectural, and must be tested by further experiments.

Since we use slab ocean models, our experiments omit the effects of ocean processes, such as circulation and deep ocean heat uptake, on the pattern of surface temperature change. We have briefly assessed these effects using a pair of experiments with HadCM3 (the computationally cheaper of our models) coupled to a dynamic ocean for 140 years. As in the slab model experiments, the cloud feedback is more negative and the climate sensitivity lower for higher-altitude forcing. The time-means of years 21–120 give similar feedbacks and patterns of T-mediated warming to the equilibrated slab experiments. Because the feedbacks are more negative in years 1–20 with the dynamic ocean model, the slab model results are quantitatively most relevant when the longer-term response dominates, as is the case for scenarios in which anthropogenic forcings roughly stabilizes in the second part of this century, but we think that the qualitative findings are applicable in any case. A detailed study with AOGCMs would be a useful subject for future studies.

Our findings highlight that equilibrium surface warming patterns cannot be explained in terms of the pattern of ESF diagnosed from AGCM runs. We speculate that this is because of coupled ocean–atmosphere feedbacks shaping the evolution of the surface warming pattern. Furthermore, our simple indices of warm pool relative forcing and warming may not fully represent the relationships between forcing pattern and climate response, as

they do not capture for example the sea-ice pattern effect (Zhou et al., 2025). The study also used highly idealized forcing structures that do not necessarily explain the responses to real forcing agents with complex spatial and temporal distributions. Future work should test the relevance of our findings to realistic forcing agents.

Conflict of Interest

The authors declare no conflicts of interest relevant to this study.

Data Availability Statement

The CESM2 and HadAM/SM3 experiment data is archived on Zenodo and can be found from the citation reference entry for Dai et al. (2025).

Acknowledgments
AZD and PC were supported by UK Research and Innovation (UKRI) under the UK government's Horizon Europe funding Guarantee (Grant EP/Y036123/1). PC was additionally supported through UK Natural Environmental Research Council Grants NE/V012045/1 and NE/T006250/1. JMG was supported by the European Research Council (ERC) under the European Union's Horizon 2020 research and innovation programme (Grant 786427, project "Couplet"). This work used JASMIN, the UK's collaborative data analysis environment (https://jasmin.ac.uk) and the ARCHER2 UK National Supercomputing Service (https://www.archer2.ac.uk).

References

Andrews, T., Forster, P. M., & Gregory, J. M. (2009). A surface energy perspective on climate change. *Journal of Climate*, *22*(10), 2557–2570. https://doi.org/10.1175/2008JCLI2759.1

Andrews, T., Gregory, J. M., & Webb, M. J. (2015). The dependence of radiative forcing and feedback on evolving patterns of surface temperature change in climate models. *Journal of Climate*, *28*(4), 1630–1648. https://doi.org/10.1175/JCLI-D-14-00545.1

Andrews, T., & Webb, M. J. (2018). The dependence of global cloud and lapse rate feedbacks on the spatial structure of tropical Pacific warming. *Journal of Climate*, *31*(2), 641–654. https://doi.org/10.1175/JCLI-D-17-0087.1

Bloch-Johnson, J., Rugenstein, M., & Abbot, D. S. (2020). Spatial radiative feedbacks from internal variability using multiple regression. *Journal of Climate*, *33*(10), 4121–4140. https://doi.org/10.1175/JCLI-D-19-0396.1

Bloch-Johnson, J., Rugenstein, M., Stolpe, M. B., Rohrschneider, T., Zheng, Y., & Gregory, J. M. (2021). Climate sensitivity increases under higher CO_2 levels due to feedback temperature dependence. *Geophysical Research Letters*, *48*(4), e2020GL089074. https://doi.org/10.1029/2020GL089074

Bloch-Johnson, J., Rugenstein, M. A. A., Alessi, M. J., Proistosescu, C., Zhao, M., Zhang, B., et al. (2024). The Green's function model intercomparison project (GFMIP) protocol. *Journal of Advances in Modeling Earth Systems*, *16*(2), e2023MS003700. https://doi.org/10.1029/2023MS003700

Bretherton, C. S., & Smolarkiewicz, P. K. (1989). Gravity waves, compensating subsidence and detrainment around cumulus clouds. *Journal of the Atmospheric Sciences*, *46*(6), 740–759. https://doi.org/10.1175/1520-0469(1989)046⟨0740:GWCSAD⟩2.0.CO;2

Caldwell, P. M., Zelinka, M. D., & Klein, S. A. (2018). Evaluating emergent constraints on equilibrium climate sensitivity. *Journal of Climate*, *31*(10), 3921–3942. https://doi.org/10.1175/JCLI-D-17-0631.1

Ceppi, P., & Gregory, J. M. (2017). Relationship of tropospheric stability to climate sensitivity and Earth's observed radiation budget. *Proceedings of the National Academy of Sciences of the United States of America*, *114*(50), 13126–13131. https://doi.org/10.1073/pnas.1714308114

Ceppi, P., & Gregory, J. M. (2019). A refined model for the Earth's global energy balance. *Climate Dynamics*, *53*(7–8), 4781–4797. https://doi.org/10.1007/s00382-019-04825-x

Ceppi, P., & Nowack, P. (2021). Observational evidence that cloud feedback amplifies global warming. *Proceedings of the National Academy of Sciences of the United States of America*, *118*(30), e2026290118. https://doi.org/10.1073/pnas.2026290118

Cess, R. D., Potter, G. L., Blanchet, J. P., Boer, G. J., Del Genio, A. D., Déqué, M., et al. (1990). Intercomparison and interpretation of climate feedback processes in 19 atmospheric general circulation models. *Journal of Geophysical Research*, *95*(D10), 16601–16615. https://doi.org/10.1029/JD095iD10p16601

Colman, R. A. (2015). Climate radiative feedbacks and adjustments at the Earth's surface. *Journal of Geophysical Research: Atmospheres*, *120*(8), 3173–3182. https://doi.org/10.1002/2014JD022896

Dai, A.-Z., Ceppi, P., & Gregory, J. (2025). Data for "Understanding the climate response to different vertical patterns of radiative forcing" (version 1) [Dataset]. *Zenodo*. https://doi.org/10.5281/ZENODO.16421789

Dong, Y., Proistosescu, C., Armour, K. C., & Battisti, D. S. (2019). Attributing historical and future evolution of radiative feedbacks to regional warming patterns using a Green's function approach: The preeminence of the western Pacific. *Journal of Climate*, *32*(17), 5471–5491. https://doi.org/10.1175/JCLI-D-18-0843.1

Forster, P., Storelvmo, T., Armour, K. C., Collins, W., Dufresne, J.-L., Frame, D., et al. (2021). The Earth's energy budget, climate feedbacks and climate sensitivity. In *Climate change 2021 – The physical science basis: Working group I contribution to the sixth assessment report of the intergovernmental panel on climate change* (pp. 923–1054). Cambridge University Press. https://doi.org/10.1017/9781009157896.009

Fueglistaler, S. (2019). Observational evidence for two modes of coupling between sea surface temperatures, tropospheric temperature profile, and shortwave cloud radiative effect in the tropics. *Geophysical Research Letters*, *46*(16), 9890–9898. https://doi.org/10.1029/2019GL083990

Gregory, J. M., & Andrews, T. (2016). Variation in climate sensitivity and feedback parameters during the historical period. *Geophysical Research Letters*, *43*(8), 3911–3920. https://doi.org/10.1002/2016GL068406

Gregory, J. M., Ingram, W. J., Palmer, M. A., Jones, G. S., Stott, P. A., Thorpe, R. B., et al. (2004). A new method for diagnosing radiative forcing and climate sensitivity. *Geophysical Research Letters*, *31*(3), L03205. https://doi.org/10.1029/2003GL018747

Günther, M., Schmidt, H., Timmreck, C., & Toohey, M. (2022). Climate feedback to stratospheric aerosol forcing: The key role of the pattern effect. *Journal of Climate*, *35*(24), 7903–7917. https://doi.org/10.1175/JCLI-D-22-0306.1

Hansen, J., Sato, M., & Ruedy, R. (1997). Radiative forcing and climate response. *Journal of Geophysical Research*, *102*(D6), 6831–6864. https://doi.org/10.1029/96JD03436

Hansen, J., Sato, M., Ruedy, R., Nazarenko, L., Lacis, A., Schmidt, G. A., et al. (2005). Efficacy of climate forcings. *Journal of Geophysical Research*, *110*(D18), D18104. https://doi.org/10.1029/2005JD005776

Held, I. M., & Shell, K. M. (2012). Using relative humidity as a state variable in climate feedback analysis. *Journal of Climate*, *25*(8), 2578–2582. https://doi.org/10.1175/JCLI-D-11-00721.1

Joshi, M. M., Gregory, J. M., Webb, M. J., Sexton, D. M. H., & Johns, T. C. (2008). Mechanisms for the land/sea warming contrast exhibited by simulations of climate change. *Climate Dynamics*, *30*(5), 455–465. https://doi.org/10.1007/s00382-007-0306-1

19448007, 2026, 1, Downloaded from https://agupubs.onlinelibrary.wiley.com/doi/10.1029/2025GL119138 by Imperial College London, Wiley Online Library on [21/10/2026]. See the Terms and Conditions (https://onlinelibrary.wiley.com/terms-and-conditions) on Wiley Online Library for rules of use; OA articles are governed by the applicable Creative Commons License

Klein, S. A., Hall, A., Norris, J. R., & Pincus, R. (2017). Low-cloud feedbacks from cloud-controlling factors: A review. *Surveys in Geophysics*, *38*(6), 1307–1329. https://doi.org/10.1007/s10712-017-9433-3

Klein, S. A., & Hartmann, D. L. (1993). The seasonal cycle of low stratiform clouds. *Journal of Climate*, *6*(8), 1587–1606. https://doi.org/10.1175/1520-0442(1993)006⟨1587:TSCOLS⟩2.0.CO;2

Knutti, R., Rugenstein, M. A. A., & Hegerl, G. C. (2017). Beyond equilibrium climate sensitivity. *Nature Geoscience*, *10*(10), 727–736. https://doi.org/10.1038/ngeo3017

Lee, J.-Y., Marotzke, J., Bala, G., Cao, L., Corti, S., Dunne, J., et al. (2021). Future global climate: Scenario-based projections and near-term information. In *Climate change 2021: The physical science basis. Contribution of working group I to the sixth assessment report of the intergovernmental panel on climate change* (pp. 553–672). Cambridge University Press.

Liu, F., Lu, J., Garuba, O., Leung, L. R., Luo, Y., & Wan, X. (2018). Sensitivity of surface temperature to oceanic forcing via q-flux Green's function experiments. Part I: Linear response function. *Journal of Climate*, *31*(9), 3625–3641. https://doi.org/10.1175/JCLI-D-17-0462.1

Liu, F., Lu, J., Garuba, O. A., Huang, Y., Leung, L. R., Harrop, B. E., & Luo, Y. (2018). Sensitivity of surface temperature to oceanic forcing via q-flux Green's function experiments. Part II: Feedback decomposition and polar amplification. *Journal of Climate*, *31*(17), 6745–6761. https://doi.org/10.1175/JCLI-D-18-0042.1

Marvel, K., Schmidt, G. A., Miller, R. L., & Nazarenko, L. S. (2016). Implications for climate sensitivity from the response to individual forcings. *Nature Climate Change*, *6*(4), 386–389. https://doi.org/10.1038/nclimate2888

Matus, A. V., & L'Ecuyer, T. S. (2017). The role of cloud phase in Earth's radiation budget. *Journal of Geophysical Research: Atmospheres*, *122*(5), 2559–2578. https://doi.org/10.1002/2016JD025951

Meyssignac, B., Chenal, J., Loeb, N., Guillaume-Castel, R., & Ribes, A. (2023). Time-variations of the climate feedback parameter are associated with the Pacific Decadal Oscillation. *Communications Earth & Environment*, *4*(1), 1–10. https://doi.org/10.1038/s43247-023-00887-2

Modak, A., & Bala, G. (2019). Efficacy of Black carbon aerosols: The role of shortwave cloud feedback. *Environmental Research Letters*, *14*(8), 084029. https://doi.org/10.1088/1748-9326/ab21e7

Modak, A., Bala, G., Cao, L., & Caldeira, K. (2016). Why must a solar forcing be larger than a CO_2 forcing to cause the same global mean surface temperature change? *Environmental Research Letters*, *11*(4), 044013. https://doi.org/10.1088/1748-9326/11/4/044013

Myers, T. A., & Norris, J. R. (2015). On the relationships between subtropical clouds and meteorology in observations and CMIP3 and CMIP5 models. *Journal of Climate*, *28*(8), 2945–2967. https://doi.org/10.1175/JCLI-D-14-00475.1

Qu, X., Hall, A., Klein, S. A., & DeAngelis, A. M. (2015). Positive tropical marine low-cloud cover feedback inferred from cloud-controlling factors. *Geophysical Research Letters*, *42*(18), 7767–7775. https://doi.org/10.1002/2015GL065627

Ramanathan, V. (1981). The role of ocean-atmosphere interactions in the CO_2 climate problem. *Journal of the Atmospheric Sciences*, *38*(5), 918–930. https://doi.org/10.1175/1520-0469(1981)038⟨0918:TROOAI⟩2.0.CO;2

Richardson, T. B., Forster, P. M., Smith, C. J., Maycock, A. C., Wood, T., Andrews, T., et al. (2019). Efficacy of climate forcings in PDRMIP models. *Journal of Geophysical Research: Atmospheres*, *124*(23), 12824–12844. https://doi.org/10.1029/2019JD030581

Rugenstein, M., Bloch-Johnson, J., Gregory, J., Andrews, T., Mauritsen, T., Li, C., et al. (2020). Equilibrium climate sensitivity estimated by equilibrating climate models. *Geophysical Research Letters*, *47*(4), e2019GL083898. https://doi.org/10.1029/2019GL083898

Salvi, P., Ceppi, P., & Gregory, J. M. (2021). Interpreting the dependence of cloud-radiative adjustment on forcing agent. *Geophysical Research Letters*, *48*(18), e2021GL093616. https://doi.org/10.1029/2021GL093616

Salvi, P., Ceppi, P., & Gregory, J. M. (2022). Interpreting differences in radiative feedbacks from aerosols versus greenhouse gases. *Geophysical Research Letters*, *49*(8), e2022GL097766. https://doi.org/10.1029/2022GL097766

Samset, B. H., & Myhre, G. (2011). Vertical dependence of black carbon, sulphate and biomass burning aerosol radiative forcing. *Geophysical Research Letters*, *38*(24), L24802. https://doi.org/10.1029/2011GL049697

Sejas, S. A., Hu, X., Cai, M., & Fan, H. (2021). Understanding the differences between TOA and surface energy budget attributions of surface warming. *Frontiers in Earth Science*, *9*, 725816. https://doi.org/10.3389/feart.2021.725816

Sherwood, S. C., Bony, S., Boucher, O., Bretherton, C., Forster, P. M., Gregory, J. M., & Stevens, B. (2015). Adjustments in the forcing-feedback framework for understanding climate change. *Bulletin of the American Meteorological Society*, *96*(2), 217–228. https://doi.org/10.1175/BAMS-D-13-00167.1

Shindell, D. T. (2014). Inhomogeneous forcing and transient climate sensitivity. *Nature Climate Change*, *4*(4), 274–277. https://doi.org/10.1038/nclimate2136

Sobel, A. H., & Bretherton, C. S. (2000). Modeling tropical precipitation in a single column. *Journal of Climate*, *13*(24), 4378–4392. https://doi.org/10.1175/1520-0442(2000)013⟨4378:MTPIAS⟩2.0.CO;2

Stevens, B., Sherwood, S. C., Bony, S., & Webb, M. J. (2016). Prospects for narrowing bounds on Earth's equilibrium climate sensitivity. *Earth's Future*, *4*(11), 512–522. https://doi.org/10.1002/2016EF000376

Stuecker, M. F., Timmermann, A., Jin, F.-F., Proistosescu, C., Kang, S. M., Kim, D., et al. (2020). Strong remote control of future equatorial warming by off-equatorial forcing. *Nature Climate Change*, *10*(2), 124–129. https://doi.org/10.1038/s41558-019-0667-6

Vial, J., Dufresne, J.-L., & Bony, S. (2013). On the interpretation of inter-model spread in CMIP5 climate sensitivity estimates. *Climate Dynamics*, *41*(11), 3339–3362. https://doi.org/10.1007/s00382-013-1725-9

Williams, A. I. L., Jeevanjee, N., & Bloch-Johnson, J. (2023). Circus tents, convective thresholds, and the non-linear climate response to tropical SSTs. *Geophysical Research Letters*, *50*(6), e2022GL101499. https://doi.org/10.1029/2022GL101499

Wilson Kemsley, S., Ceppi, P., Andersen, H., Cermak, J., Stier, P., & Nowack, P. (2024). A systematic evaluation of high-cloud controlling factors. *Atmospheric Chemistry and Physics*, *24*(14), 8295–8316. https://doi.org/10.5194/acp-24-8295-2024

Wood, R., & Bretherton, C. S. (2006). On the relationship between stratiform low cloud cover and lower-tropospheric stability. *Journal of Climate*, *19*(24), 6425–6432. https://doi.org/10.1175/JCLI3988.1

Zelinka, M. D., Klein, S. A., & Hartmann, D. L. (2012). Computing and partitioning cloud feedbacks using cloud property histograms. Part II: Attribution to changes in cloud amount, altitude, and optical depth. *Journal of Climate*, *25*(11), 3736–3754. https://doi.org/10.1175/JCLI-D-11-00249.1

Zhang, Y., & Fueglistaler, S. (2020). How tropical convection couples high moist static energy over land and ocean. *Geophysical Research Letters*, *47*(2), e2019GL086387. https://doi.org/10.1029/2019GL086387

Zhou, C., Wang, M., Zelinka, M. D., Liu, Y., Dong, Y., & Armour, K. C. (2023). Explaining forcing efficacy with pattern effect and state dependence. *Geophysical Research Letters*, *50*(3), e2022GL101700. https://doi.org/10.1029/2022GL101700

Zhou, C., Wang, Q., Tan, I., Zhang, L., Zelinka, M. D., Wang, M., & Bloch-Johnson, J. (2025). Sea ice pattern effect on Earth's energy budget is characterized by hemispheric asymmetry. *Science Advances*, *11*(9), eadr4248. https://doi.org/10.1126/sciadv.adr4248

19448007, 2026, 1, Downloaded from https://agupubs.onlinelibrary.wiley.com/doi/10.1029/2025GL119138 by Imperial College London, Wiley Online Library on [21/10/2026]. See the Terms and Conditions (https://onlinelibrary.wiley.com/terms-and-conditions) on Wiley Online Library for rules of use; OA articles are governed by the applicable Creative Commons License

Zhou, C., Zelinka, M. D., & Klein, S. A. (2016). Impact of decadal cloud variations on the Earth's energy budget. *Nature Geoscience*, *9*(12), 871–874. https://doi.org/10.1038/ngeo2828

Zhou, C., Zelinka, M. D., & Klein, S. A. (2017). Analyzing the dependence of global cloud feedback on the spatial pattern of sea surface temperature change with a Green's function approach. *Journal of Advances in Modeling Earth Systems*, *9*(5), 2174–2189. https://doi.org/10.1002/2017MS001096

19448007, 2026, 1, Downloaded from https://agupubs.onlinelibrary.wiley.com/doi/10.1029/2025GL119138 by Imperial College London, Wiley Online Library on [21/10/2026]. See the Terms and Conditions (https://onlinelibrary.wiley.com/terms-and-conditions) on Wiley Online Library for rules of use; OA articles are governed by the applicable Creative Commons License